JOURNAL OF EXPERIMENTAL AND THEORETICAL PHYSICS, 2024, Vol. 166, No. 6 (12), pp. 739–752

ATOMS, MOLECULES, OPTICS

DISINTEGRATION DYNAMICS OF A WATER MOLECULE IN AN INTENSE HIGH-FREQUENCY FIELD

© 2024 *A. V. Bibikov*[a*], *S. N. Yudin*[a], *M. M. Popova*[a], *M. D. Kiselev*[a,b,c], *A. N. Grum-Grzhimailo*[a,c], *E. V. Gryzlova*[a]

[a] *Skobeltsyn Institute of Nuclear Physics, Moscow State University, Moscow, 119991 Russia*

[b] *Pacific National University, Khabarovsk, 680035 Russia*

[c] *School of Physics and Engineering, ITMO University, Saint Petersburg, 197101 Russia*

[*] *e-mail: bibikov@sinp.msu.ru*

Received May 16, 2024

Revised May 16, 2024

Accepted September 10, 2024

Abstract. As result of the development of sources of intense high-frequency radiation and the improvement of techniques for detecting charged fragments, experiments on multiple ionization of inner molecular shells with the momentum and charges of fragmentation products being registered in coincidence have become possible. In this paper, the dynamics of the disintegration of water molecule fragments resulting from interaction with intense X-ray radiation has been studied. The charge distribution of oxygen ions was calculated, Newton diagrams were con-structed for fragments — protons and the oxygen ion — at various charge states of the latter, and the kinetic energy release was determined. Calculations were performed using the original code [1] for parameters close to the experiment [2] conducted on EuXFEL in 2021.

DOI: 10.31857/S004445102412e010

1. INTRODUCTION

The study of the water molecule, due to its abundance in the Universe and its significance for biology, are of particular practical interest for the physics of the interaction of small quantum objects with radiation. Information on the water molecule evolution, i.e. the fraction of formed ions and radicals, in an ionizing electromagnetic field is critical for applications such as the study of radiation damage in X-ray diffraction experiments, the chemistry of radicals in solutions [3, 4] and even for the explanation of some phenomena occurring in the atmospheres of planets [5, 6] and comets [7].

When an atom or a molecule interacts with X-rays, usually first occurring event is photoemission. In most cases, the loss of the first electron does not lead to the decay of the molecule, since the amount of the remaining electrons in the valence shell may be sufficient to form a molecular bond, particularly due to the fact that ionization from the inner K shell dominates in the high-frequency range. The resulting hole state quickly relaxes due to Auger decay or, in contrast, an even more excited state is formed due to subsequent photoemission. Thus, the first act of ionization triggers a complex chain of competing processes, such as fluorescence, Auger decay, dissociation, and, finally, the Coulomb explosion of the molecule, and the evolution of a sample depends on the field parameters, intensity, duration, polarization, etc. [8, 9]. In some cases, the system may end up completely devoid of electrons [10].

Auger process in the water cation H_2O^+ with a K-vacancy (SCH, single core hole) were studied theoretically and experimentally [11–13]. The calculations predicted an unfolding of the cation bond angle to 120° and a lifetime of about 5 fs. The water dication H_2O^{2+} has not been observed in a stable state, but it is efficiently formed during Auger decay of an inner vacancy [14] or, for example, during double ionization [15]. The dissociation of the water dication in lower excited states was studied in [16, 17]. The similarity of the Auger spectra corresponding to the decay of a $1s$ vacancy localized on the oxygen atom for various oxygen-containing molecules was discussed in [18].

If the radiation intensity is high, then a dication with double vacancy on the K-shell (DCH, double core hole) is able to be formed. The features of the Auger decay of the DCH molecular ion were first discussed in [19] and have since been the subject of numerous studies — see, for example, the review [20]. The first calculation of the spectra of Auger electrons with a single and double vacancy in the inner shell [21] showed that nuclear dynamics in DCH, unlike SCH, has a strong influence on the electron emission spectra, and its lifetime is only about 2 fs.

One of the problems of experiments in the gas phase is the random orientation of the molecule in space, that leads to averaging and, as a consequence, blurring of the many physical effects. Coincidence measurements of photoelectrons and charged fragments make it possible to determine the axis (orientation) of the molecule in space, which, in particular, allows to observe features of the angular distributions of photoelectrons that are indistinguishable in the traditional setup [22]. The measuring in Coincidence significantly complicates the collection of statistics and, accordingly, increases the requirements for detector sensitivity. As a result of such experiments, the characteristics of the processes taking place are recorded in more details, permitting connecting electronic and nuclear dynamics [23, 24]: for example, it was shown how measuring the angular distributions in a molecular system 'fixed' using a coincidence experiment allows one to determine molecular bond length [25] or even to determine through which dissociation channel the molecule was disintegrated [26, 27].

The development of methods for theoretical description of the angular distributions of photoelectrons at the ionization of molecules has started with the work [28], and since then, a variety of methods have been used to describe the states of the continuous spectrum: from R-matrix [29] and the numerical solution of the Schrödinger equation [30] to the currently very popular XCHEM approach [31].

This work is stimulated by the experiment studying the dynamics of the disintegration of a water molecule, carried out in 2021 at the European X-ray free-electron laser EuXFEL, where the momenta of protons produced as a result of the Coulomb explosion of the molecule were measured along with the momentum and charge state of the oxygen ion [2].

Unless otherwise specified, the atomic system of units is used.

2. BASIC PRINCIPLES OF THE THEORETICAL METHOD

The interaction of a molecule with electromagnetic field can cause various chains of events, which we will call *trajectories*. A simplified evolution of a water molecule, including configuration states and their geometry, is presented in Figure 1. The first event when a water molecule H_2O is irradiated with synchrotron radiation is necessarily ionization, and ionization of the $1s$ shell is one and a half orders of magnitude more probable than ionization of the valence shell. The geometry of the H_2O^+ ion (cation) differs from the geometry of a neutral molecule by a slightly larger (by $\sim 10^\circ$) opening angle, regardless of whether ionization has occurred from the inner $ph(i)$ or the valence $ph(v)$ shell. The further trajectory, on the contrary, cruciality depends on where the vacancy occurs.

If ionization occurs from the inner shell ph(i), then the geometry of the molecule, determined by the position of the nuclei, does not have enough time to rearrange itself and Auger decay (au) occurs with a characteristic time of about 5 fs into a doubly charged ion H_2O^{2+} (dication), the equilibrium configuration of which is a linear molecule. A significant deviation of the nuclear positions in the neutral H_2O molecule and in the H_2O^{2+} molecular ion leads to excitation of scissoring, symmetric and asymmetric vibration modes. If the radiation intensity is high, i.e. there is the probability that second ionization of the inner shell occurs before Auger decay, then a molecular ion with a double K vacancy is formed. As our calculations showed, DCH does not have an equilibrium state and quickly decays.

If ionization occurs from the valence shell, then the H_2O^+ ion gently relaxes into a configuration that is equilibrium for a singly charged ion, and the second ionization is possible. Note that two trajectories of approximately equal probability $ph(i) - ph(v)$ and $ph(v) - ph(i)$ ((b) and (c) in Figure 1, correspondingly) lead to the same state with a single vacancy in $1s$-shell, for which there is also a dissociation channel into fragments HO^+ and H^+, although at a lower rate than for the DCH state.

Trajectories $ph(i) - au$ and $ph(v) - ph(v)$ ((d) and (e) in Figure 1, correspondingly) lead to the most stable of the water dications in its ground configuration, but the next ionization event, regardless of the shell, leads to a Coulomb explosion of the molecule.

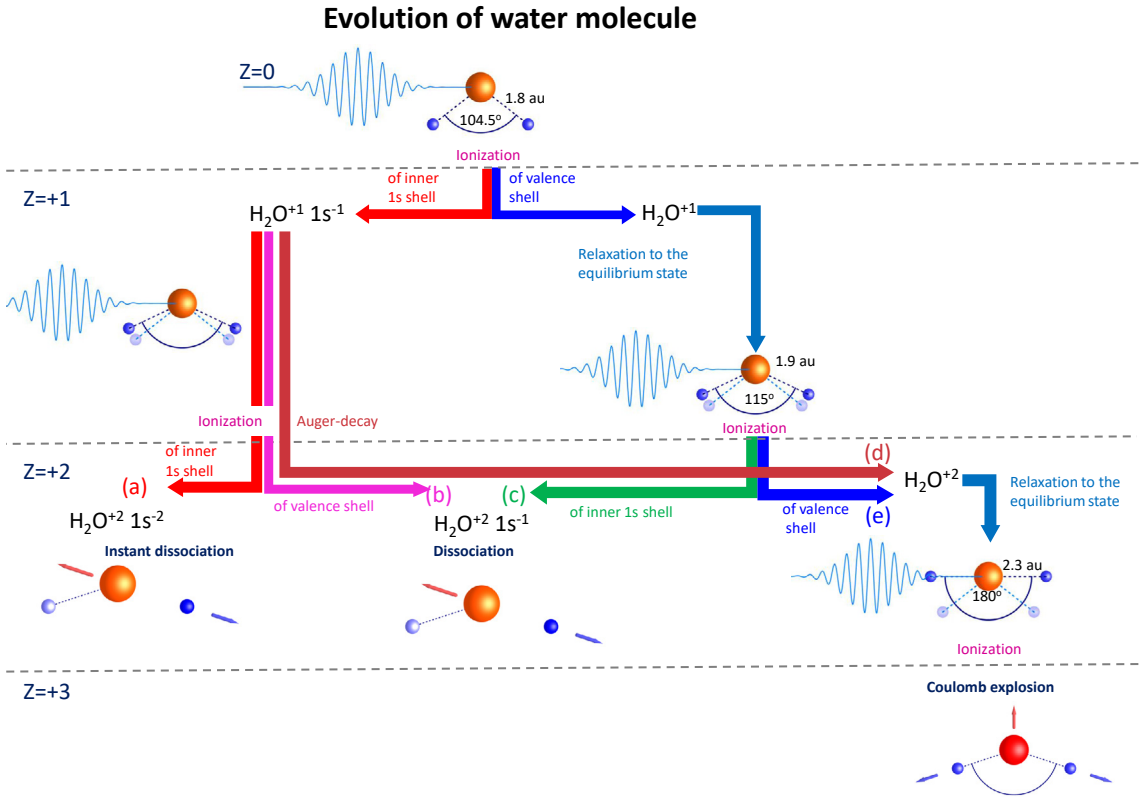

Fig. 1. Water molecule evolution in an intense electromagnetic field.

We simulate the quantities according to the measurements made in the work [2]: the charge distribution of oxygen ions, the kinetic energy released by the fragments of the molecule as a result of Coulomb repulsion, and the momentum distribution of the molecule fragments measured in coincidence.

Below, we will consider the following aspects of the approach in more detail: in section 2.1 we present the equations of classical particle motion in the potential describing the disintegration dynamics; in paragraph 2.2 we consider quantum-chemical aspects: potential energy surfaces and vibration frequencies; in 2.3 we discuss the probabilities of the various trajectories occurring.

2.1. Dynamics of the charged fragments disintegration

According to the stated in the previous paragraph, we accept the following model of the H_2O molecule destruction under the influence of high-intensity radiation in order to find the spatial trajectories of atoms — fragments of the molecule. Before the molecular ion reaches $Z = +2$ charge state, the atoms are placed in the configuration of neutral water, experiencing zero-point oscillations relative to the equilibrium position. This is justified by the fact that the equilibrium configuration of the $+1$ molecular ion is close to the equilibrium configuration of neutral water (see paragraph 2.2). To determine the time evolution of the position of the atomic nuclei of a molecular ion H_2O^{2+}, the equations of classical motion in a potential are solved:

$$\begin{aligned}
\frac{d\mathbf{p}_1}{dt} &= -\partial_{r_{01}}\mathcal{P}\frac{\mathbf{r}_{01}}{r_{01}} - \partial_f\mathcal{P}\left(\frac{\mathbf{r}_{02}}{r_{01}r_{02}} - f\frac{\mathbf{r}_{01}}{r_{01}^2}\right),\\
\frac{d\mathbf{p}_2}{dt} &= -\partial_{r_{02}}\mathcal{P}\frac{\mathbf{r}_{02}}{r_{02}} - \partial_f\mathcal{P}\left(\frac{\mathbf{r}_{01}}{r_{01}r_{02}} - f\frac{\mathbf{r}_{02}}{r_{02}^2}\right),\\
\frac{d\mathbf{p}_0}{dt} &= -\frac{d\mathbf{p}_1}{dt} - \frac{d\mathbf{p}_2}{dt}.
\end{aligned} \tag{1}$$

Here $\mathcal{P}$ is the potential energy surface (PES), $\mathbf{p}_{0,1,2}$ — the momenta of the oxygen ion and each of the hydrogen atoms, respectively. For a planar triatomic molecule, the potential energy surface is a function of the two vector's lengths and the angle between them. For a water molecule, it is natural to choose the radius vectors from the oxygen atom to the hydrogen atoms (r_{01}, r_{02}) and angle θ between them:

$$\begin{aligned}
\mathcal{P} &= V\left(r_{01}, r_{02}, f\right),\\
f &= \cos\theta = \frac{\mathbf{r}_{01}\cdot\mathbf{r}_{02}}{r_{01}r_{02}}.
\end{aligned} \tag{2}$$

The potential energy surface is calculated by quantum chemical software packages (see paragraph 2.2), and for a system with a charge $Z \geq +3$ or at asymptotically large distances it transforms into a Coulomb repulsion potential.

As a result of modeling the system (1), the momenta of protons and oxygen ions are determined. They can be presented in different forms; for easier comparison with the experiment, we follow the representation used in [2], namely, in the form of Newton diagrams. Fig. 2a shows the scheme for constructing a Newton diagram for the disintegration of a water molecule: the momenta of protons and an oxygen ion of a specific charge Q are determined in coincidence, the momentum of oxygen is plotted along the x axis, and the momenta of protons are shown relatively to this direction.

Figure 2b shows the Newton diagram calculated in the simplest model, where the initial conditions for the numerical solution of system (1) are determined by the equilibrium geometry of the neutral water molecule, and the PES for the system with charge $Z = +3$ is reduced to the Coulomb potential. The resulting plot is far from the experimental one, discussed in detail in Section 3. Therefore, below, for the system with charge $+2$, we use quantum-chemical PES, and randomly generated coordinates and momenta of the atoms of the H_2O molecule, corresponding to the probability distribution of zero-point oscillations of the harmonic oscillator (see paragraph 2.2), are chosen as the initial conditions for the numerical solution of system (1).

As mentioned above, the PES of the H_2O^+ cation in any configuration differs slightly from the PES of neutral water. The PES of the dication H_2O^{2+}, on the contrary, differs significantly from the PES of neutral water and depends on the electronic configuration. We consider three cases: DCH, SCH and two vacancies in the valence shell (ground state of dication). We do not take into account PES with excited valence electrons, since the lower excited PES slightly differs from the ground state PES.

Further ionization into the $+3$ state leads to purely Coulomb disintegration of charged fragments of the molecule, i.e. the equations of motion (1) remain the same, but $\mathcal{P}$ is replaced by the Coulomb potential. At this stage of the numerical solution, each fragment is set a charge of $+1$. Thus, for dissociation channel $O^+ + H_2^+$ the possibility of transition into the $O^{2+} + H_2^+$ state is lost. We emphasize that quantum chemical calculations predict that the contribution of such a channel is insignificant (see paragraph 2.2). After the disintegration and until the end of the electromagnetic pulse, the possibility of further evolution of the charge state of the oxygen ion accounts.

2.2. Quantum chemical basis of the approach

For the water cation and dication $H_2O^{+,2+}$ we performed PES calculations using the original code [1,32–35] tested on calculations of BeO, $Be(OH)_2$ crystalls and more complex molecules $Be@C_{36}$. The energy of electrons in the field of three heavy nuclei of the H_2O molecule was calculated in the unrestricted Hartree-Fock (UHF) approximation, taking into account electron-electron correlations in the second order of perturbation theory (MP2). An extended set of molecular basis functions quadruple zeta aug-cc-pVQZ, which takes into account correlations and valence polarization, was used [36, 37]. To control the calculation results, some of them were

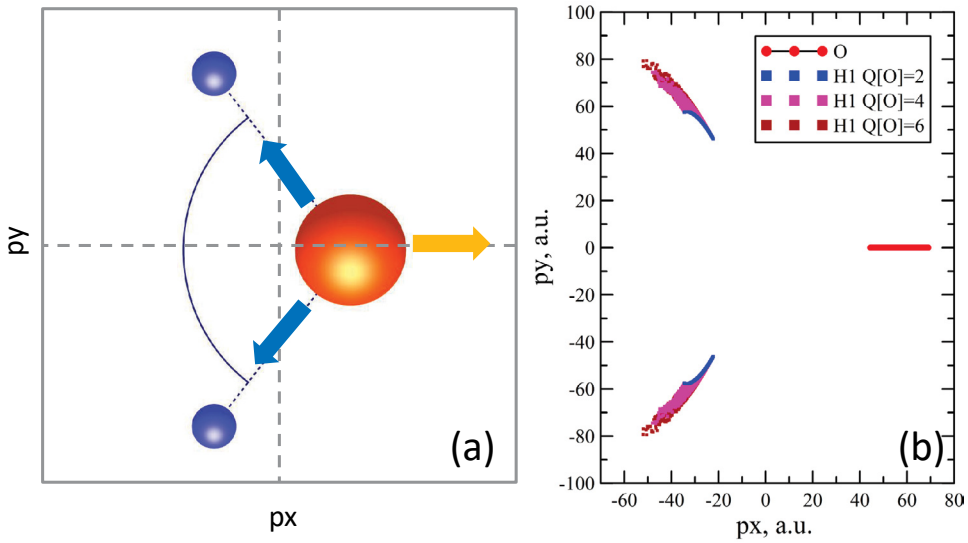

Fig. 2. (a) Newton diagram for three-particle disintegration of a molecule; (b) Newton diagram calculated in the simplest model of Coulomb three-particle disintegration of a water molecule.

compared with those calculated using the GAMESS software package using the ROHF method, taking into account correlations using the MP2 method in the aug-cc-pVQZ basis.

Figure 3 shows the results of PES calculations for the H_2O^+ cation and H_2O^{2+} dication of water. The symbols represent the calculation results, and the solid curves are the fitting with a combination of the Morse and Coulomb potentials. The curves corresponding to the symmetric arrangement of hydrogen atoms ($r_1 = r_2$) and for a fixed position of one of the atoms are shown. Figure 3 a,b shows the calculations for the cation in the ground state and with a vacancy in the $1s$ shell. It can be seen that both for symmetric and for asymmetric deviations of hydrogen nuclei from the equilibrium state, a significant potential well is formed, which ensures the equilibrium configuration. Figure 3 c,d,e shows the PES for the H_2O^{2+} dication of water in the ground state, with a single vacancy in the $1s$ shell (SCH) and with a double vacancy (DCH). Figures 3 a-e are shown for the optimal angle between the directions to the hydrogen atoms (115° for the cation and 180° for the dication). Figure 3f shows the PES (Fig. 3e) for the optimal distance between the hydrogen atoms as a function of the angle between them.

As the analysis of the PES calculations with one or two vacancies on the $1s$ shell shows (Fig. 3 d,e), there is no bound state for such a water dication, and dissociation occurs via the asymmetric channel (magenta curve) into the OH^+ and H^+ fragments. For the ground state of the dication (Fig. 3 c), even for the asymmetric vibration mode, there is a small barrier of 0.1 eV (magenta curve). This barrier is lower than the zero-point energy of neutral water, therefore the molecule dissociates, which is consistent with the conclusions of [38]. Thus, the motion of the system along the blue curves is responsible for the dissociation channel into $O + 2H^+$, and along the magenta and brown curves — into $H^+ + OH^+$. The dissociation to the asymmetric channel $H^+ + OH^+$ is prevailed, which is consistent with the results of [39].

The table 1 shows the frequencies of scissor (scis), symmetric (sym) and asymmetric (asym) oscillations for various water ions. We have identified the frequency component corresponding to the harmonic oscillator (harm), the anharmonic frequency (anh), the cubic (cub) and biquadratic (qu) corrections to the harmonic frequency. A significant anharmonicity of symmetric and asymmetric modes is observed, which increases noticeably for the SCH state. Note that for the dication, the ratio of the frequencies of the radial modes changes — the rigidity of the symmetric mode becomes higher than that of the asymmetric one. For the SCH-state, the asymmetric mode becomes unstable, the symmetric mode exists on the edge of the calculation error (marked with an asterisk), and for the DCH-state, the bound state is completely absent.

The calculations given in the table 1 are in reasonable agreement with the experimental data [11]: 1645, 3831, 3944 cm^{-1} for neutral water, and 3710, 1121 cm^{-1} for a cation with a K-vacancy. A slight change in

Table 1. Vibrational frequencies of neutral water, its cation and dication [cm^{-1}]

	$H_2O(Z=+2)$					$H_2O(Z=+2)1s^{-1}$				$H_2O(Z=+1)1s^{-1}$				$H_2O(Z=0)$			
Mode	GAMESS	harm	anh	cub	qu	harm	anh	cub	qu	harm	anh	cub	qu	harm	anh	cub	qu
scis	686	677	729	13	38	735	718	-7	-10	1314	1249	-69	4	1626	1608	-21	3
sym	1673	1679	957	-998	276	907	-4*	-437	-474	3603	3404	-418	218	3846	3673	-363	190
asym	1144	1155	533	-1111	489	-	-	-	-	3628	3427	-441	240	3973	3807	-369	203

the equilibrium state of the neutral molecule and cation ($\sim 10^\circ$) is also in agreement with experiment and calculations [11].

As mentioned in paragraph 2.2, the position and momentum of hydrogen atoms oscillate. For neutral water, there is no physically defined initial moment of time. Therefore, the oscillations for each mode are taken into account randomly with a Gaussian distribution of width related to the frequencies by the ratio $\sqrt{m_i\omega_i}$ and $1/\sqrt{m_i\omega_i}$ for the coordinate and momentum, respectively [40] (m_i is the reduced mass of the hydrogen atom). For example, the amplitude of radial oscillations is estimated to be approximately equal to 0.3 au, i.e. it is a significant (about 15%) correction to the equilibrium bond length. The momentum transferred by a photon to the oxygen atom (about 6 a.u.) can cause oscillations in the center-of-mass system with an energy of $2 \cdot 10^{-4}$ a.u., which is one and a half orders of magnitude less than the energies of the lowest excited states of the water molecule associated with the motion of nuclei (see the table 1).

For further analysis it is important to understand whether the water dication has time to turn from the 105° position, which is the equilibrium position for neutral water, to the 180° position, which characterizes the equilibrium for the water dication. The characteristic turnaround time is approximately 10 fs, which for the electromagnetic field under consideration (see paragraph 2.3) is close to the time of second photoionization.

2.3. Charge state of oxygen

The evolution of a water molecule charge configuration and its fragments along a specific trajectory is simulated using a developed analogue of a genealogical scheme incorporating the probabilities of atomic transitions (photoionization, Auger transitions, radiative transitions [19]). This simplified approach is considered justified when one studies ionization by high-frequency radiation, in the domain where the probabilities of the processes reach asymptotic behavior [41, 42]. The probability of ionization of various shells of the atom and oxygen ions were obtained using the Herman-Skillman algorithm [43] and is in a complete agreement with the calculations [44,45]. The Auger decay and fluorescence probabilities were taken from [42]. The Auger decays can be classified according to the $2s$ (L) and valence (V) electrons involved as (LL), (LV), and (VV). The probability of the first of these is almost the same as the probability of Auger decay of the oxygen ion. The Auger decay rates (in a.u.) of the SCH state used in this study $7.01 \cdot 10^{-4}$ (LL), $1.36 \cdot 10^{-3}$ (LV), $2.04 \cdot 10^{-3}$ (VV) and of the DCH states $2.164 \cdot 10^{-3}$ (LL), $4.62 \cdot 10^{-3}$ (LV), $6.39 \cdot 10^{-3}$ (VV) differ from corresponding ones given in [21] $1.51 \cdot 10^{-4}$, $1.4 \cdot 10^{-3}$, $3.8 \cdot 10^{-3}$, and $7.65 \cdot 10^{-4}$, $3.6 \cdot 10^{-3}$, $11.6 \cdot 10^{-3}$, however the total width for these two calculations is in reasonable agreement. The systematically smaller width of the VV-channel, when the photo- and active electrons belong to the valence shell, is associated with the absence of interatomic Auger decay in our model.

A multi-electron atom, such as oxygen, can form ions of different charges, from O^+ to O^{8+}, and many different configurations can correspond to an ion of the same charge. It should be emphasized that, under certain conditions, some exotic «hollow» configurations (for example, O^{6+}, $1s^0 2s^2$) can be formed with a higher probability than the ground states of a given ion [8].

The charge configuration is determined at each time interval based on the probability of transition from the current state to the next by the Monte Carlo method — by generating a random number with a constant probability

$$P(a \to b) = w_{a\to b} dt$$

for Auger decay and fluorescence, and with the time-dependent photoionization probability

$$P(a \to b) = j(t)\sigma_{a\to b} dt.$$

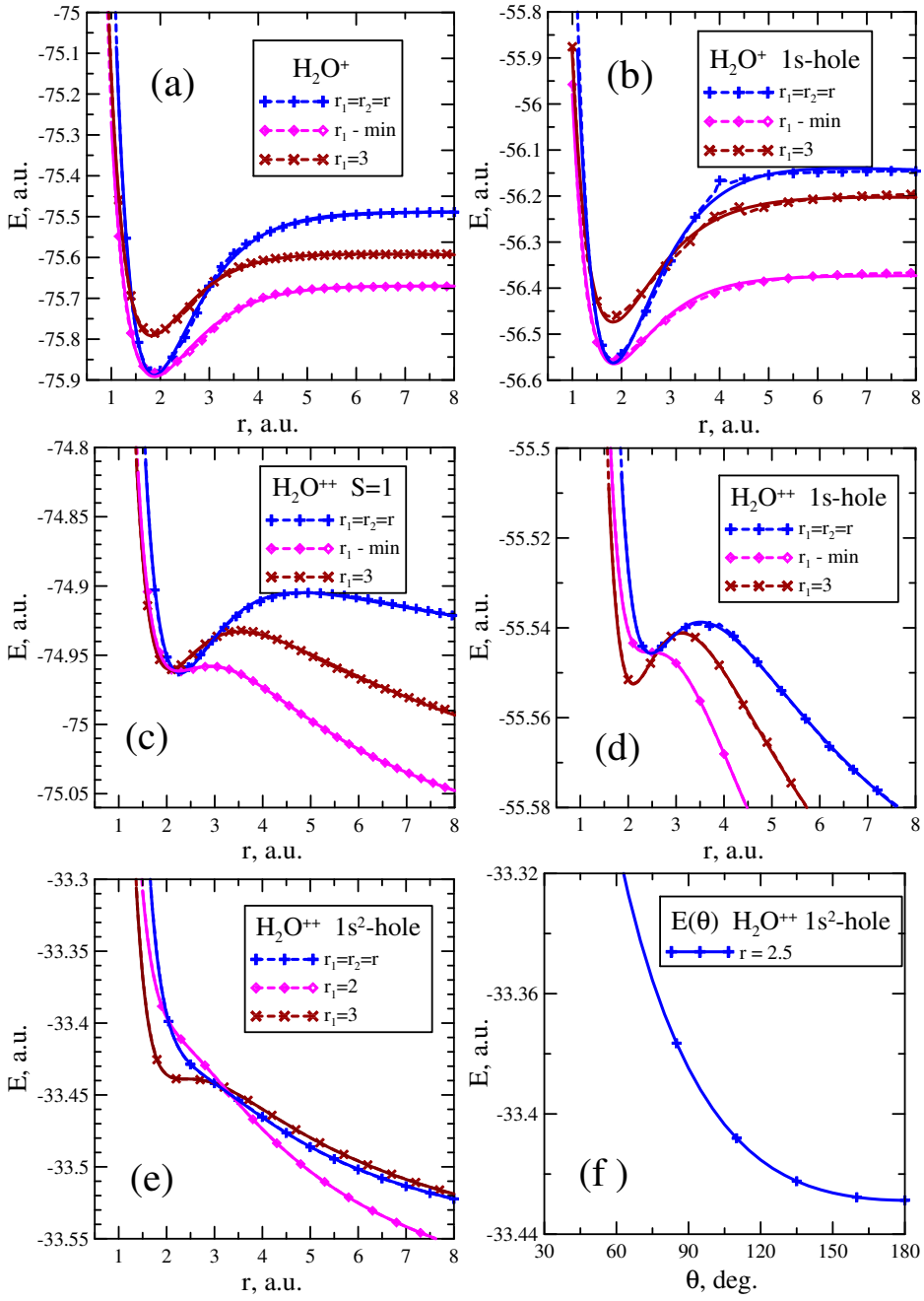

Fig. 3. The section of the potential energy surface of the water ions H_2O^+ and H_2O^{2+}: (a,b) single charged ion H_2O^+ in the ground state and with a $1s$ vacancy localized on the oxygen atom; (c-e) a doubly charged ion H_2O^{2+} in the ground state (c), with one (d) and two (e) vacancies in the $1s$ shell at a fixed angle; (f) the case presented in (e) at fixed proton coordinates as a function of the angle between the directions to them. The different curves correspond to different deviations from the equilibrium position: symmetrical arrangement of hydrogen atoms ($r_1 = r_2$, blue curve), the fixed position of one of the atoms in the minimum potential energy (r_1 - min, magenta curve) and in $r_1 = 3$ a.u. (brown curve). The dots show the results of calculations, the solid curves are the result of their fitting by a combination of Morse and Coulomb potentials

Here $w_{a\to b}$ is the transition rate from configuration a to configuration b, $\sigma_{a\to b}$ is the photoionization cross section, $j(t)$ — flux density of the radiation. In such a way, the number of disintegration trajectories required to reach satisfactory statistics (100000 - 250000) is collected.

The real envelope of the electromagnetic pulse is difficult to determine, and is approximated using cosine functions or a Gaussian distribution. The parameters that are considered to be specified are the fluence – the integral flux of photons in the pulse, and the width (full width at half-maximum — FWHM). For most of the calculations, we used radiation pulses of the following shape:

$$j(t) = j_0 \cos^4(\pi\, t/t_p)\,, \tag{3}$$

where j_0 is the amplitude of the flux density in the pulse, t_p is the total duration of the pulse. The characteristic duration of pulses generated by free electron lasers are about 10–25 fs FWHM [46, 47]. For pulse (3) fluence F for photons with energy E_γ:

$$F = 3\, t_p\, j_0/8E_\gamma\,. \tag{4}$$

One can distinguish the basic trajectories of the molecule evolution that start with the ionization of the inner shell (fig. 1):

a. $ph(i) \to ph(i) \to$ instantaneous dissociation $(Z = +2)$;

b. $ph(i) \to ph(v) \to$ dissociation $(Z = +2)$;

c. $ph(v) \to ph(i) \to$ dissociation $(Z = +2)$;

d. $ph(i) \to au \to ph(i, v) \to$ Coulomb explosion $(Z = +3)$;

e. $ph(v) \to ph(v) \to ph(i, v) \to$ Coulomb explosion $(Z = +3)$.

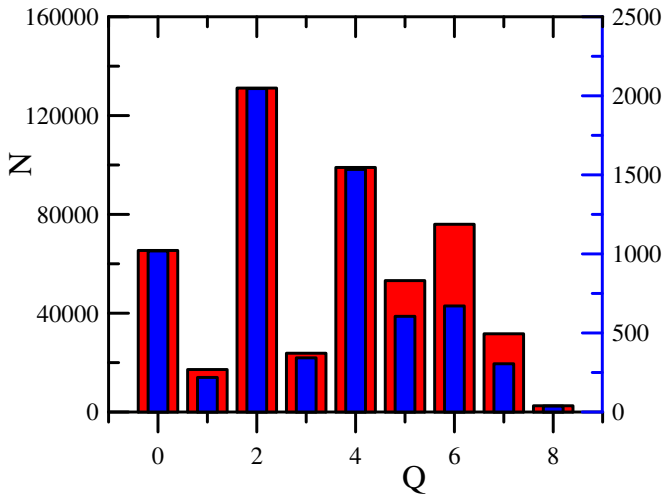

Fig. 4. The charge distribution of oxygen ion yields calculated for a pulse with a photon energy of 1000 eV, fluence $2 \cdot 10^{11}$ photons/μm^2, and duration 40 fs. Red bars correspond to the present calculations (left scale), blue one to the calculations from [2] (right scale)

In figure 4 the results of our calculations of oxygen yields N of various charges Q in comparison with the calculations of [2] are shown. The previously noted [48] prevailed formation of ions with even charges is observed, since the trajectories $ph(i) - au$ — ionization of the inner shell with subsequent Auger decay — are realized with a higher probability. The slightly greater formation of ions with $Z > 4$ that we obtained indicates, likely, to a slightly larger effective pulse length.

3. RESULTS AND DISCUSSION

3.1. The Newton diagrams

Figure 5 shows the results of calculations of the momenta of protons and the oxygen ion O^{2+} with various initial conditions for solving the system of equations (2): (a) – the initial state is determined by the equilibrium geometry of a neutral water molecule; (b) – the initial state is random and is determined by its scissor vibrations; (c) – the same, but for the symmetrical vibrations; (d) – the same, but for the asymmetrical vibrations; (e) – taking into account all three vibration modes for neutral water.

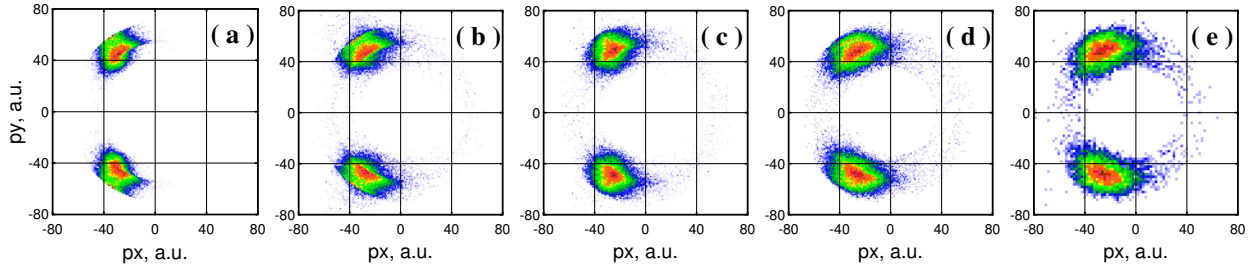

Fig. 5. The Newton diagrams for protons measured in coincidence with the oxygen ion O^{2+} for different modes allowed for the initial state of the neutral water molecule H_2O: (a) – the equilibrium configuration; (b) – only scissoring oscillations are allowed; (c) – only symmetrical oscillations are allowed; (d) – only asymmetrical oscillations are allowed; (e) – the scissoring, symmetrical and asymmetrical oscillations are allowed.

A specific and important feature of the measurements performed in [2] is a noticeable number of protons detected in the same hemisphere with the oxygen ion. For this to become possible in principle, it is necessary for the molecular ion to detach from a highly unfolded configuration, when the angle between the directions to the hydrogen atoms is close to 180°, and in this case the ion must be significantly asymmetrical. It can be shown that during the decay of a water molecule from a symmetrical geometry, the hydrogen ion cannot escape to the forward half-plane with respect to the oxygen ion. Therefore, for events to occur in the forward half-plane, the presence of an asymmetric mode is necessary. Unlike the symmetrical and scissoring vibrations, which arise due to the difference in the equilibrium geometries of neutral water and the dication, the asymmetrical oscillations, although automatically accounting in calculations with the quantum-chemical PES, cannot be excited if they were not present in the neutral molecule. Therefore, such events are not observed in Fig. 5a. It can be seen that taking into account the zero-point oscillations of the neutral water molecule solves this problem.

3.2. The influence of the oxygen evolution on disintegration dynamics

To study the difference between early and late disintegration of a molecule, in Fig. 6, we have provided a comparison of the Newton diagrams for protons measured in coincidence with oxygen ions of different charge states O^{2+}, O^{4+} and O^{6+}. The oxygen ions in these charge states prevail at the end of the pulse (see Fig. 4). Obviously, events with a higher charge correspond to earlier ionization of neutral water and faster decay of the molecular ion. This leads to a decrease in the number of protons registered in the same hemisphere with oxygen and an increase in the average momentum of protons, which was observed in the experiment and confirmed by the calculations.

Figure 7 represents the integral of the Newton diagrams in Fig. 6, namely, the total number of events with a given total kinetic energy of fragments. Ions of lower charge correspond to curves shifted to the low-energy region, and ions of higher charge correspond to curves shifted to the high-energy region. The difference in the acquired kinetic energy for ions with $\Delta Z = 2$ is of the order of 10 eV. The blue curve in Fig. 7, corresponding to a lower charge, undergoes fewer statistical fluctuations and is more sensitive to the pulse shape, while the green curve, corresponding to a higher charge, is significantly averaged (smeared). Fig. 7b shows the calculations for a pulse of a more complex shape: the sum of a narrow (10 fs) and a wide (50 fs) pulse with an intensity ratio of 1:1.

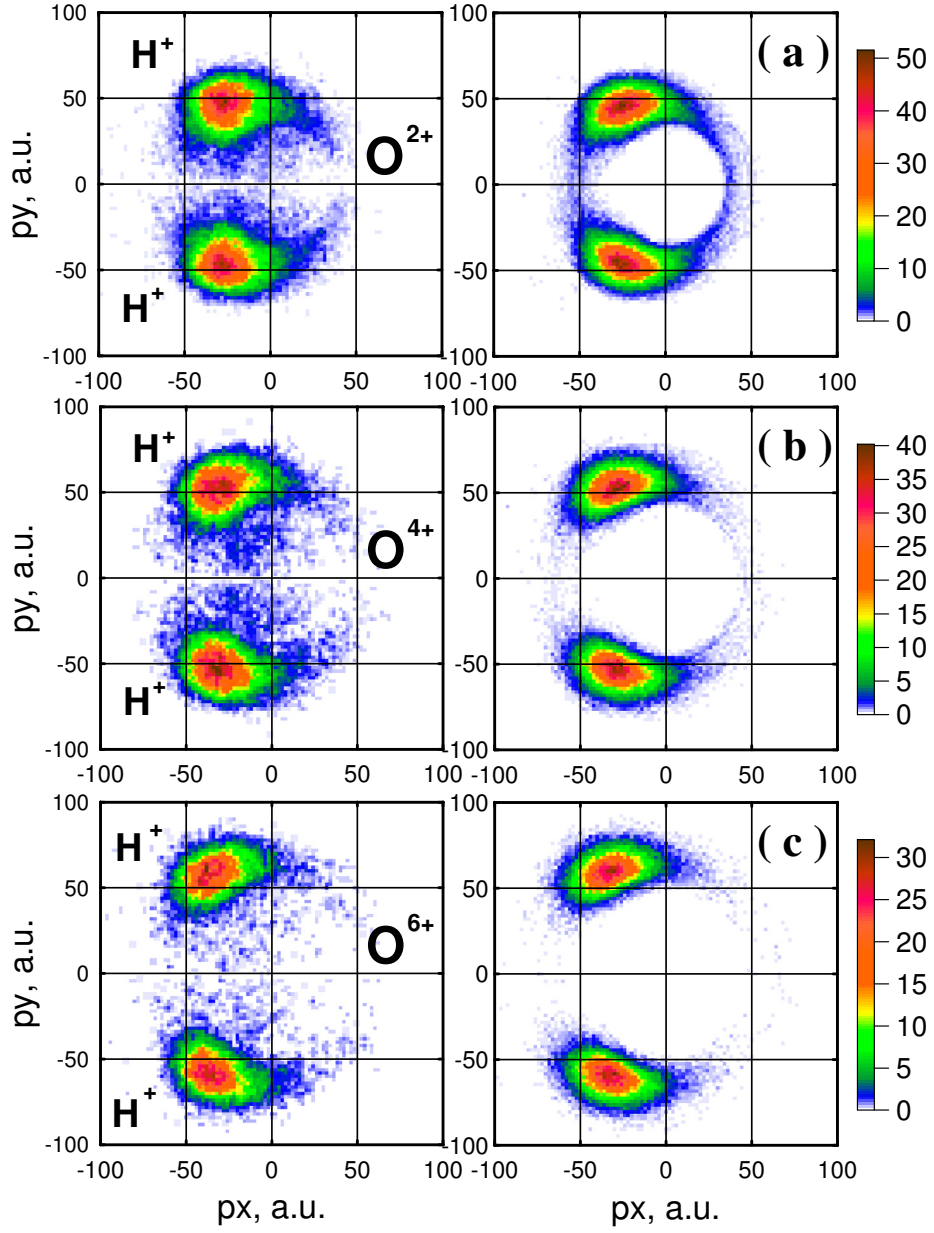

Fig. 6. The Newton's diagrams for protons detected in coincidence with oxygen ion O^{2+} (a), O^{4+} (b), and O^{6+} (c). On the left — the experimental data [2], on the right — the calculation results

3.3. Photoelectron spectra

Figure 8 shows the spectra of electrons emitted when a water molecule is irradiated with intense electromagnetic radiation. The different curves correspond to the different charges of the oxygen (ion) from which the electron is emitted. The group of lines in the region of 900-950 eV corresponds to photoemission from the valence shells, the group of lines 300-600 eV includes both photoemission lines from the inner K-shell and Auger electrons. The black line at 460 eV corresponds to K-shell ionization of neutral water molecule. We emphasize that the difference in the ionization potential of this shell in an oxygen atom (536 eV) and a water molecule (539 eV), is beyond the resolution of the supposed detector, for which the resolution of $0.01E_e$ is considered very good (E_e — electron energy). All lines located lower in energy than this photopeak correspond to photoionization of the K-shell, with the $1s^1 \to 1s^0$ branch dominating for a singly charged ion, and $1s^2 \to 1s^1$ for a doubly charged

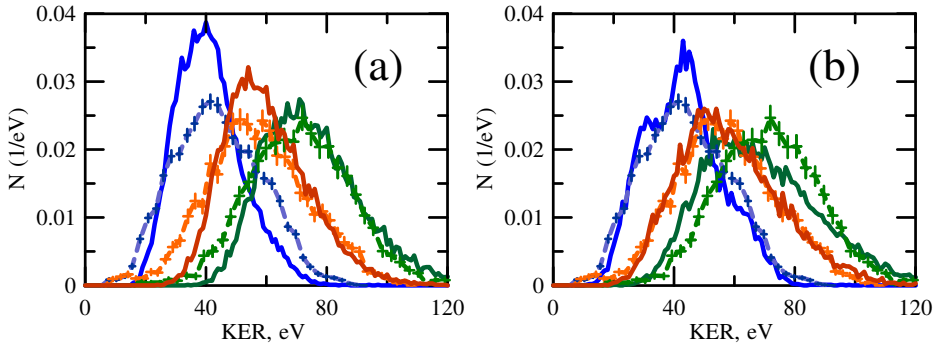

Fig. 7. The kinetic energy release (KER) for O^{2+} ions is blue lines, O^{4+} is red lines and O^{6+} is green lines. The experimental data [2] are shown with dots with errors and a dashed line, the solid lines correspond to the current calculations: (a) for a pulse of the shape (3), (b) for a pulse of a more complex shape, namely the sum of narrow (10 fs) and wide (50 fs) pulses with an intensity ratio of 1:1

ion. This is explained by the lack of ions in the corresponding initial state, namely, single-charged ions mainly have a K-vacancy, and in doubly-charged ones it is already filled due to the Auger decay. Structures higher in energy than the photopeak 460 eV correspond to the Auger electrons. The trident structure observed for the Auger spectrum of an ion of fixed charge is due to the participation of two $2s$ electrons LL (lower energy), one $2s$ electron and one valence electron V, and two valence electrons VV (higher energy) in the decay. The structure of the Auger spectrum we predicted is in accordance with the calculations of [18].

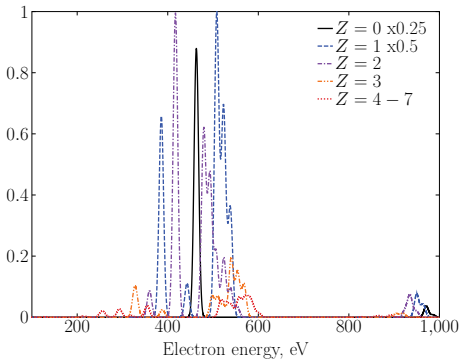

Fig. 8. Photoelectron spectrum of the water ionization by a pulse with photon energy 1000 eV with fluence $2 \cdot 10^{11}$ ph/μm^2 and duration 40 fs. The contributions from the ionization of a neutral ($Z = 0$) and singly charged ($Z = 1$) water molecule are decreased relative to the other contributions by the factor 4 and 2 respectively.

4. CONCLUSION

In the paper we considered the dynamics of water molecule fragments disintegration initiated by interaction with an intense electromagnetic pulse. The charge distribution of oxygen ions is obtained, and the acquired final momenta of protons and oxygen at the end of the molecule decay are simulated for different charge trajectories of the molecule. The results are presented in the form of the Newton diagrams, that is, the diagrams of proton momenta measured in the coincidence with the momentum of oxygen. The kinetic energy release (KER) acquired due to the Coulomb explosion of the molecule is calculated. All calculations were performed for conditions relevant to the experiment [2], and compared with the results presented there. The agreement of experimental data and calculations shows the applicability of the proposed method.

The calculated and measured Newton diagrams show maxima and a tail of events corresponding to a proton emitted in the same hemiplane as the oxygen ion. While the main maxima are formed due to Coulomb three-particle disintegration, the tail is formed by the various vibrational modes of a neutral water molecule, its cation and dication. Calculations have shown a significant sensitivity of the kinetic energy release to the shape of the electromagnetic pulse.

5. ACKNOWLEDGMENTS

The development of an approach to describe the dynamics of the water molecule disintegration, the compilation of the corresponding Newton diagrams and the analysis of the potential energy surfaces of water ions were carried out with the financial support of the Ministry of Science and Higher Education of the Russian Federation, grant No. 075-15-2021-1353. The analysis of photoelectron spectra during ionization of a water molecule was supported by the Russian Science Foundation, project No. 23-62-10026 [49]. The computational part was supported by the Ministry of Science and Higher Education of the Russian Federation within the framework of project No. FEME-2024-0005.

The authors would like to thank Professors Renaud Guillemin and Marc Simon for providing the original experimental data from the work [2].

REFERENCES

1. A. Artemyev, A. Bibikov, V. Zayets, and I. Bodrenko, J. Chem. Phys. **123**, 024103, (2005).

2. T. Jahnke et al. Phys. Rev. X **11**, 041044 (2021).

3. B. Boudaiffa, P. Cloutier, D. Hunting, M. A. Huels, and L. Sanche, Science **287**, 1658 (2000).

4. B. C. Garrett et al., Chem. Rev. **105**, 355 (2005).

5. R. W. Carlson et al., Science **283**, 2062 (1999).

6. M. Blanc, D. J. Andrews, A. J. Coates, D. C. Hamilton, C. M. Jackman, X. Jia, A. Kotova, M. Morooka, H. T. Smith, and J. H. Westlake, Space Sci. Rev. **192**, 237 (2015).

7. I. G. Draganic, Radiat. Phys. Chem. **72**, 181 (2005).

8. S. Serkez, G. Geloni, S. Tomin, G. Feng, E. V. Gryzlova, A. N. Grum-Grzhimailo, and M. Meyer, J. Opt. **20**, 024005 (2018).

9. E. V. Gryzlova, M. D. Kiselev, M. M. Popova, and A. N. Grum-Grzhimailo, Phys. Rev. A **107**, 013111 (2023).

10. F. Braube, Phys. Rev. A **97**, 043429 (2018).

11. A. Sankari, C. Stråhlman, R. Sankari, L. Partanen, J. Laksman, J. A. Kettunen, I. F. Galvin, R. Lindh, P.-Å. Malmqvist, and S. L. Sorensen, J. Chem. Phys. **152**, 074302 (2020).

12. H. Siegbahn, L. Asplund, and P. Kelfve, Chem. Phys. Lett. **35**, 330 (1975).

13. H. Ågren and O. Vahtras, J. Phys. B **26**, 913 (1993).

14. A. Moddeman, J. A. Carlson, M. O. Krause, B. P. Pullen, W. E. Bull, and G. K. Schweitzer, J. Chem. Phys. **55**, 2317 (1971).

15. S. W. J. Scully, Phys. Rev. A **73**, 040701R (2006).

16. Z. L. Streeter, F. L. Yip, R. R. Lucchese, B. Gervais, T. N. Rescigno, and C.W. McCurdy, Phys. Rev. A **98**, 053429 (2018).

17. D. Reedy et al., Phys. Rev. A **98**, 053430 (2018).

18. P. Wang, T. X. Carroll, T. D. Thomas, L. J. Søthre, K. J. Børve, J. Electron Spectros. Relat. Phenomena **251**, 147103 (2021).

19. L. S. Cederbaum, F. Tarantelli, A. Sgamellotti, and J. Schirmer, J. Chem. Phys. **85**, 6513 (1986).

20. M. N. Piancastelli, Eur. Phys. J. Special Topics **222**, 2035 (2013).

21. L. Inhester, C. F. Burmeister, G. Groenhof, and H. Grubmüller, J. Chem. Phys. **136**, 144304 (2012).

22. R. Dorner, V. Mergel, O. Jagutzki, L. Spielberger, J. Ullrich, R. Moshammer, and H. Schmidt-Böcking, Phys. Rep. **330**, 95 (2000).

23. M. N. Piancastelli, A. Hempelmann, F. Heiser, O. Gessner, A. Rüdel, and U. Becker, Phys. Rev. A **59**, 300 (1999).

24. A. Sankari, C. Stråhlman, R. Sankari, L. Partanen, J. Laksman, J. A. Kettunen, I. F. Galván, R. Lindh, P.-Å. Malmqvist, and S. L. Sorensen, J. Chem. Phys. **152**, 074302 (2020).

25. H. Fukuzawa et al., J. Chem. Phys. **150**, 174306 (2019).

26. T. Severt, Z. L. Streeter, W. Iskandar, K. A. Larsen, A. Gatton, D. Trabert, B. Jochim, B. Griffin, E. G. Champenois, M. M. Brister, D. Reedy, D. Call, R. Strom, A. L. Landers, R. Dörner, J. B. Williams, D. S. Slaughter, R. R. Lucchese, T. Weber, C. W. McCurdy, and I. Ben-Itzhak, Nat. Commun. **13**, 5146 (2022).

27. J. Howard, M. Britton, Z. L. Streeter, C. Cheng, R. Forbes, J. L. Reynolds, F. Allum, G. A. McCracken, I. Gabalski, R. R. Lucchese, C. W. McCurdy, T. Weinacht, and P. H. Bucksbaum, Commun. Chem. **6**, 81 (2023).

28. D. Dill and J. L. Dehmer, J. Chem. Phys. **61**, 692 (1974).

29. L. Moore, M. Lysaght, L. Nikolopoulos, J. Parker, H. van der Hart, and K. Taylor, J. Mod. Opt. **58**, 1132 (2011).

30. R. R. Lucchese, K. Takatsuka, and V. McKoy, Phys. Rep. **131**, 147 (1986).

31. C. Marante, M. Klinker, I. Corral, J. Gonzalez-Vazquez, L. Argenti, and F. Martin, J. Chem. Theory Comput. **13**, 499 (2017).

32. E. V. Tkalya, A. V. Bibikov, and I. V. Bodrenko, Phys. Rev. C **81**, 024610, (2010).

33. E. V. Tkalya, A. V. Avdeenkov, A. V. Bibikov, I. V. Bodrenko, and A. V. Nikolaev, Phys. Rev. C **86**, 014608, (2012).

34. A. V. Bibikov, A. V. Avdeenkov, I. V. Bodrenko, A. V. Nikolaev, and E. V. Tkalya, Phys. Rev. C **88**, 034608, (2013).

35. A. V. Bibikov, G. Y. Korenman, and S. N. Yudin, Moscow Univ. Phys. **78**, 107 (2023).

36. T. H. Dunning, J. Chem. Phys. **90**, 1007 (1989).

37. K. L. Schuchardt, B. T. Didier, T. Elsethagen et al., J. Chem. Inf. Model. **47**, 1045 (2007), doi:10.1021/ci600510j

38. B. Gervais, E. Giglio, L. Adoui, A. Cassimi, D. Duflot, and M. E. Galassi, J. Chem. Phys. **131**, 024302 (2009).

39. H. B. Pedersen et al., Phys. Rev. A **87**, 013402 (2013).

40. L. D. Landau and E. M. Lifshitz, *Course of Theoretical Physics, Vol. 3. Quantum Mechanics: Non-Relativistic Theory* (Elsevier, Amsterdam, 2013; Fizmatlit, Moscow, 2004).

41. V. Y. Lunin, A. N. Grum-Grzhimailo, E. V. Gryzlova, D. O. Sinitsyn, T. E. Petrova, N. L. Lunina, N. K. Balabaev, K. B. Tereshkina, A. S. Stepanov, Y. F. Krupyanskii, Acta Cryst. D **71** , 293 (2015).

42. Kengo Moribayashi, J. Phys. B **41**, 085602 (2008).

43. F. Herman and S. Skillman, *Atomic Structure Calculations*, Englewood Cliffs: Prentice-Hall Inc. (1963).

44. J. J. Yeh and I. Lindau, Atomic Data and Nuclear Data Tables **32**, 1 (1985).

45. Sang-Kil Son, L. Young, and R. Santra, Phys. Rev. A **83**, 033402 (2011).

46. E. Allaria, R. Appio, L. Badano et al., Nat. Phot. **6**, 699 (2012).

47. P. Finetti et al., J. Opt. **19**, 114010 (2017).

48. C. Buth, R. Beerwerth, R. Obaid, N. Berrah, L. S. Cederbaum, and S. Fritzsche, J. Phys. B **51**, 055602 (2018).

49. https://rscf.ru/en/project/23-62-10026/.